Supporting Online Materials:

Hydrophobic Nanoparticle-Based Nanocomposite Films Using *In Situ* Ligand Exchange Layer-by-Layer Assembly and Their Nonvolatile Memory Applications

Yongmin Ko, Hyunhee Baek, Younghoon Kim, Miseon Yoon and Jinhan Cho*

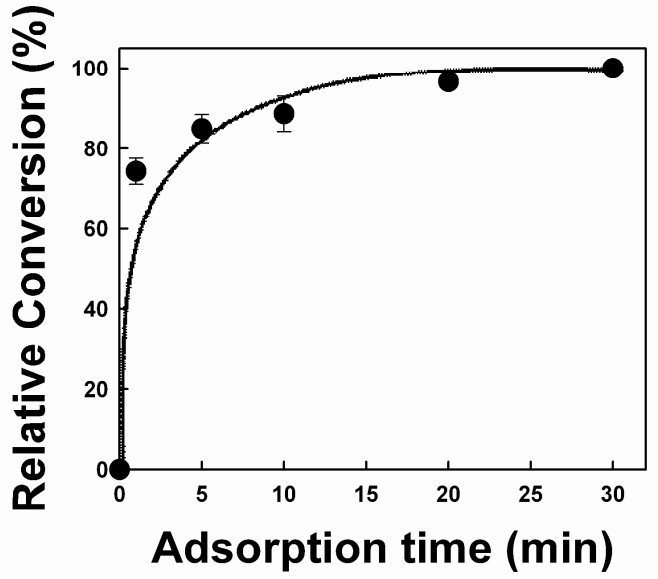

Figure S1. Degree of relative conversion of the Ag_{NP} ligands from the PA stabilizers to the dendrimers at the outermost PA-Ag_{NP} layer, as a function of the dendrimer adsorption time. The relative conversion rate was calculated by comparing the ATR-FTIR absorption peak area of palmitic acid groups (at 1740 cm^{-1}) as a function of dendrimer adsorption time (see Figure 1A). In this case, a 0% conversion rate indicates the presence of palmitic acid bound to the Ag_{NPs} when the outermost layer comprises PA-Ag_{NP}. A 100% conversion rate indicates that the PA ligands were completely replaced by the dendrimer when the outermost layer comprises the dendrimer. The solid lines are drawn as a guide for the eye.

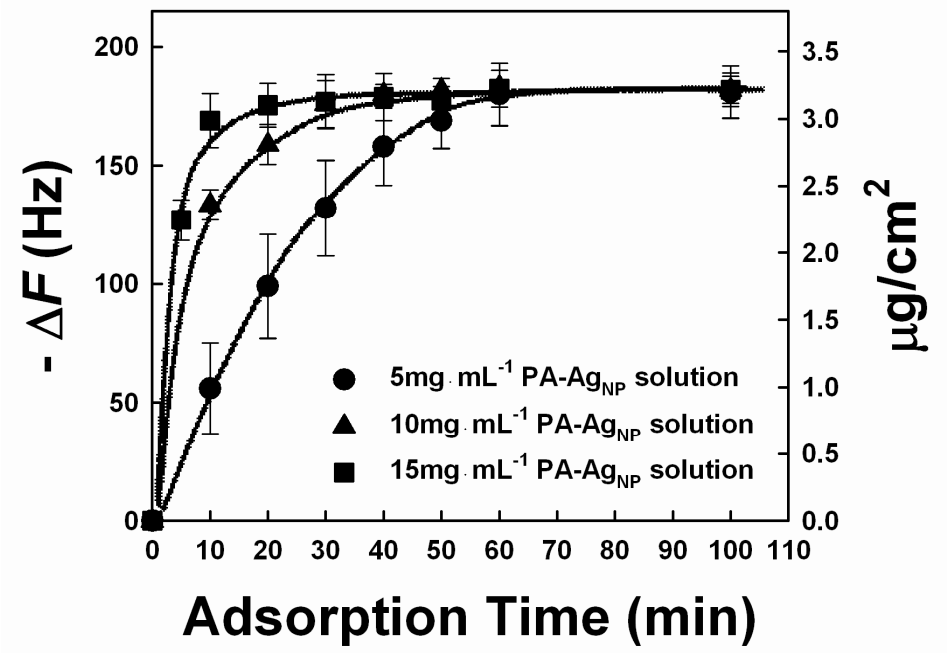

Figure S2. Adsorption isotherm behavior for PA-Ag_{NP} onto a dendrimer-coated QCM electrode as a function of solution concentration and adsorption time. The solid lines were drawn as a guide for the eye.

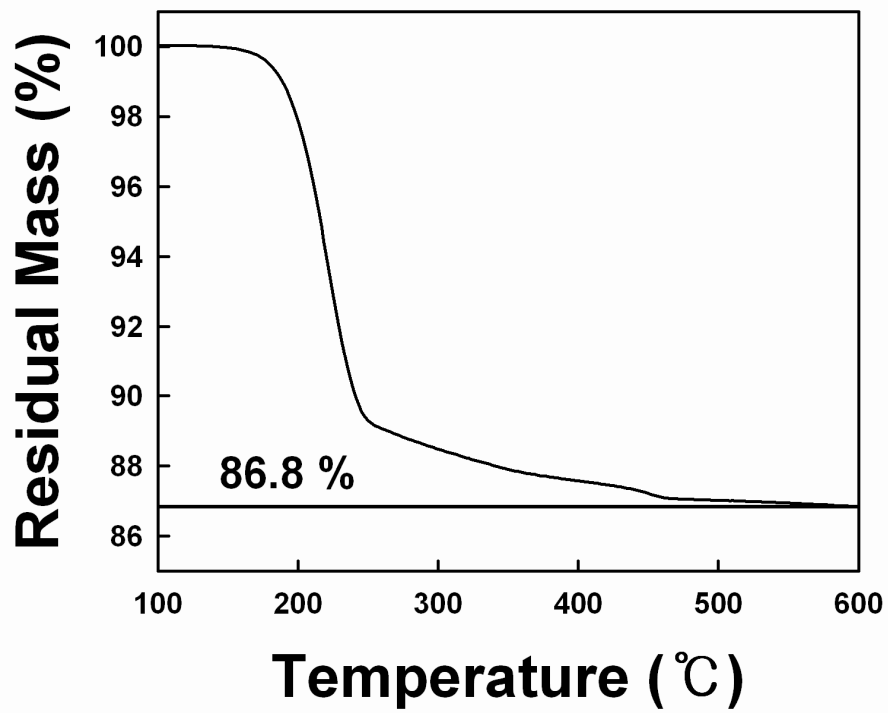

Figure S3. Thermogravimetric analysis (TGA) of the dendrimer/PA-Ag_{NP} multilayer films. The TGA heating rate was 10°C/min.

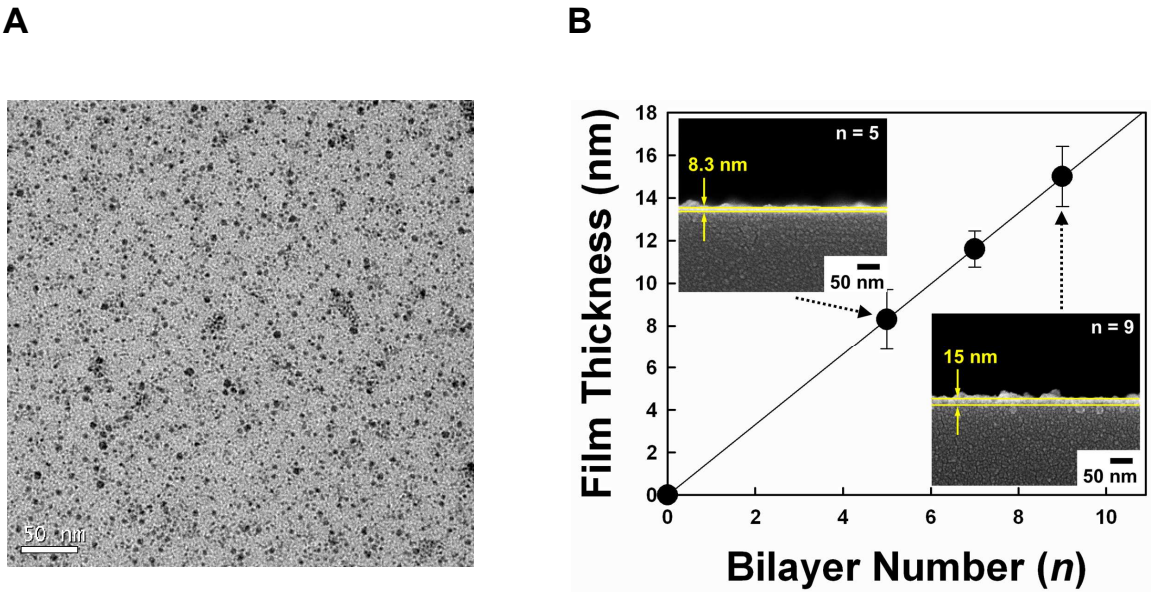

Figure S4. (A) HR-TEM image of a mercaptoacetic acid (MAA)-stabilized Ag_{NP} single layer adsorbed onto a cationic dendrimer-coated TEM grid. (B) Film thickness of the (cationic dendrimer/anionic MAA-stabilized Ag_{NP})$_9$ multilayers. MAA-Ag_{NPs} dispersed in water were prepared using the phase transfer of PA-Ag_{NPs} from toluene to aqueous media. The MAA-Ag_{NP} and dendrimer solution pH were adjusted to 3.5 and 7.5, respectively. The solution concentrations of MAA-Ag_{NP} and the dendrimer during electrostatic LbL deposition were identical to those of the PA-Ag_{NP} and dendrimer used during the preparation of the ISLE-LbL films. The thickness per electrostatic bilayer was measured to be about 1.66 nm.

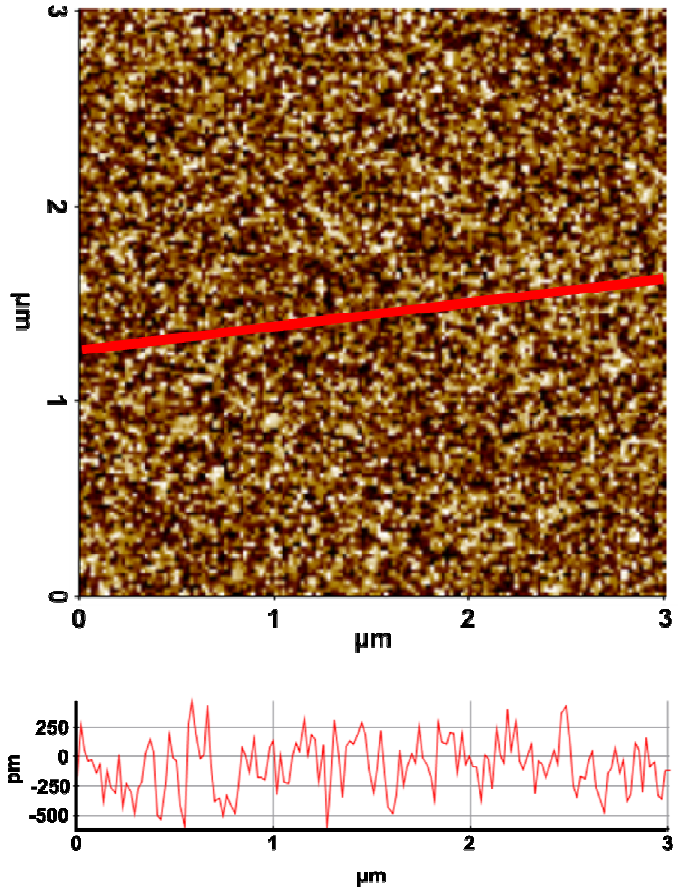

Figure S5. AFM image of a single dendrimer layer deposited onto a silicon wafer. The root-mean-square (RMS) surface roughness and the peak-to-valley height of dendrimer monolayer were measured to be about 0.13 nm and 1 nm, respectively.

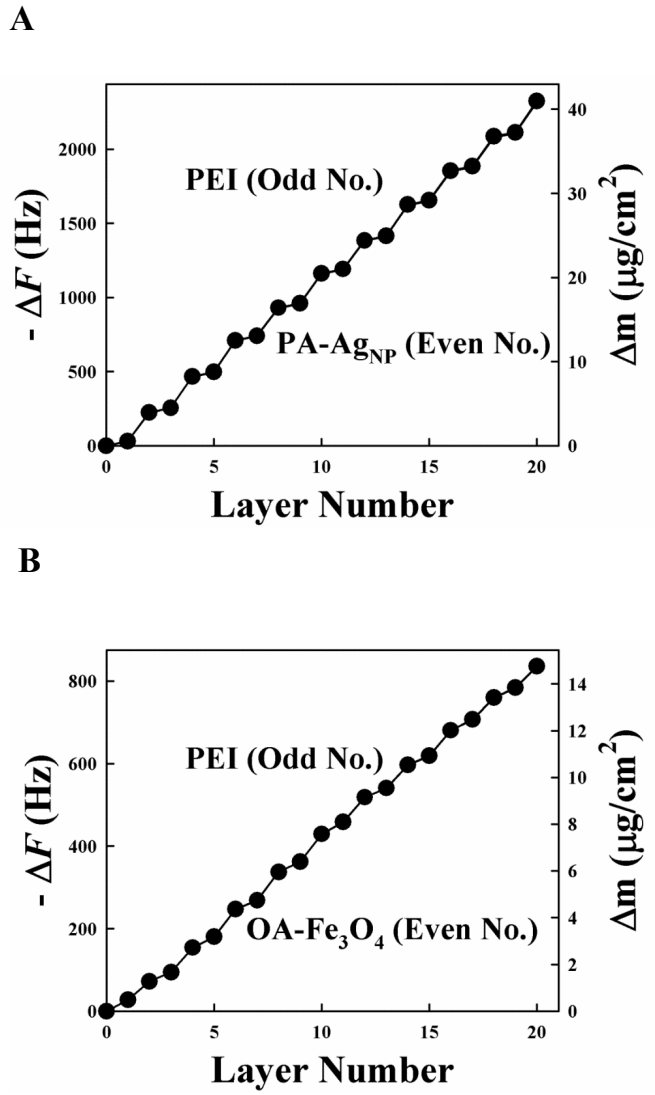

Figure S6. (A) QCM data of $(PEI/PA\text{-}Ag_{NP})_n$ and (B) $(PEI/OA\text{-}Fe_3O_4)_n$ as a function of layer number.

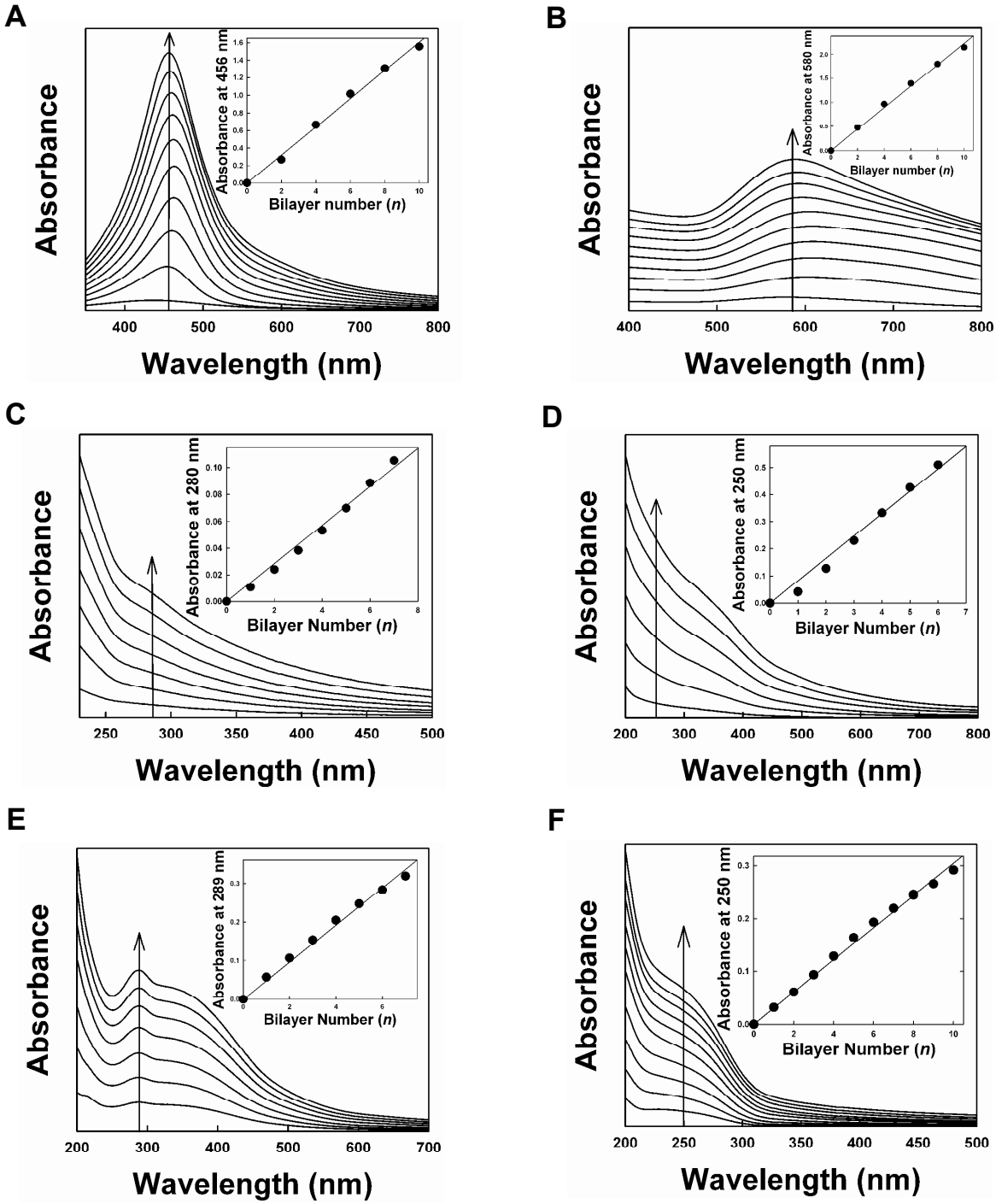

Figure S7. UV-vis spectra of (A) (dendrimer/PA-Ag_{NP})$_n$, (B) (dendrimer/TOA-Au_{NP})$_n$, (C) (dendrimer/TOA-Pd_{NP})$_n$, (D) (dendrimer/OA-Fe_3O_4)$_n$, (E) (dendrimer/TOA-MnO_2)$_n$, (F) (dendrimer/OA-$BaTiO_3$)$_n$ multilayers as a function of bilayer number (n). The insets indicate the UV-vis absorbance of (dendrimer/hydrophobic NP)$_n$ multilayers as a function of bilayer number.

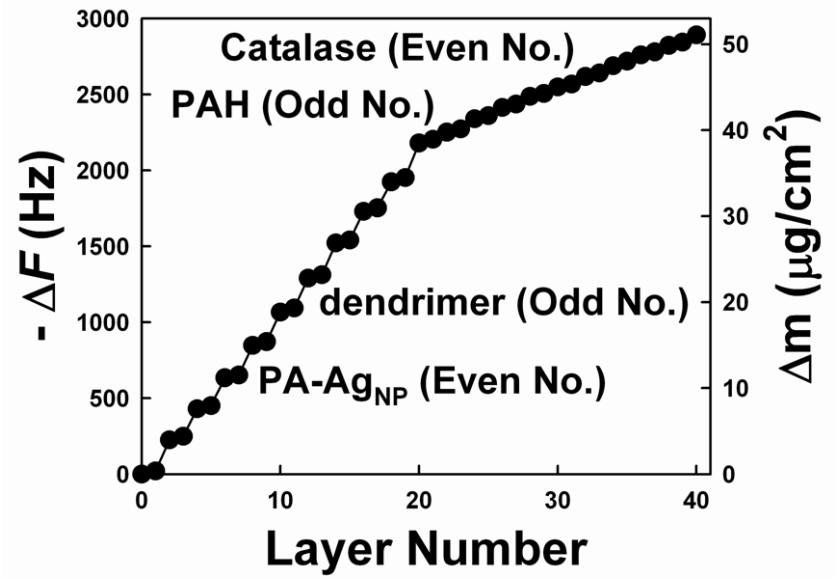

Figure S8. QCM mass measurements during the electrostatic LbL assembly of (PAH/catalase)$_n$ multilayers deposited onto ligand exchange-induced (dendrimer/PA-Ag$_{NP}$)$_n$ multilayers. The PAH and catalase solution pH values were adjusted to pH 9 for the positively charged PAH and the negatively charged catalase.

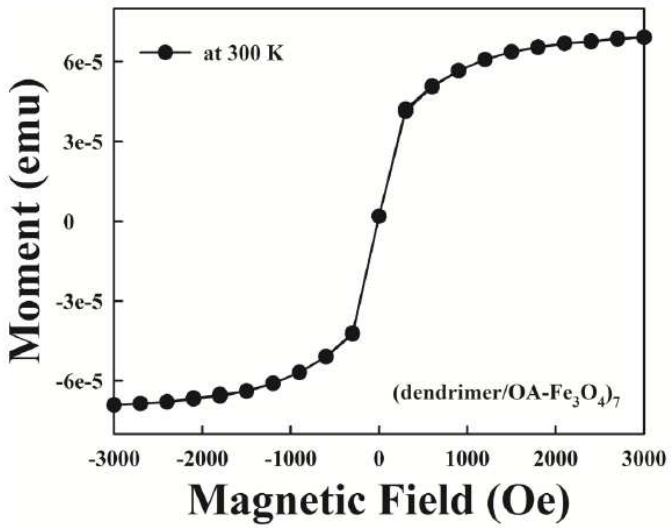

Figure S9. The magnetic curves of (dendrimer/OA-Fe_3O_4)$_7$ multilayer-coated silicon wafer measured at 300 K.

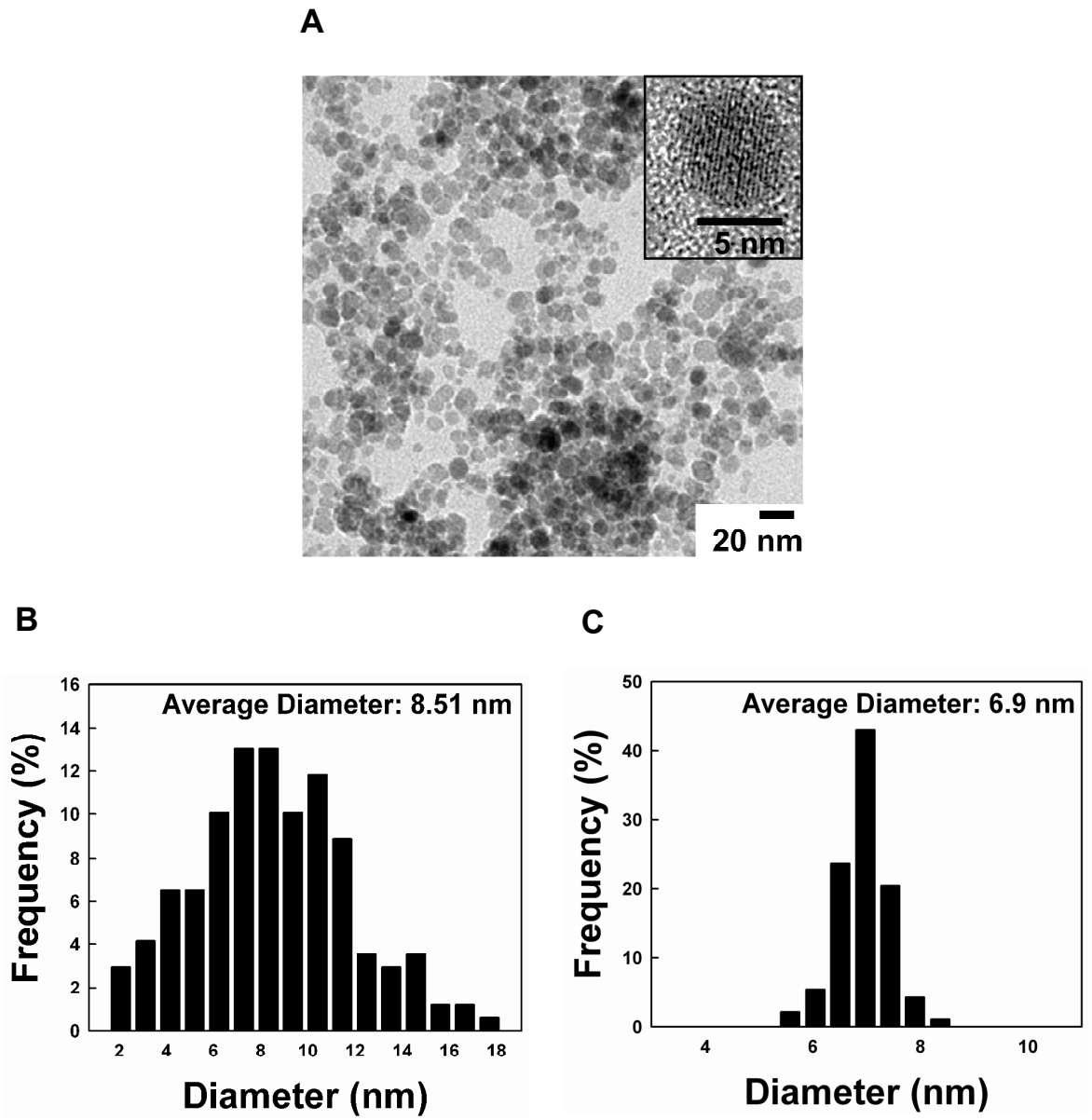

Figure S10. (A) HR-TEM image of Fe_3O_4 synthesized in aqueous solution. The inset indicate lattice image of aqueous Fe_3O_4 NP. The particle size distribution analyses of (B) aqueous anionic Fe_3O_4 NPs and (C) OA-Fe_3O_4 NPs. Here, the size distribution histogram of OA-Fe_3O_4 NPs prepared in toluene is shown for comparison with the anionic Fe_3O_4 NPs synthesized in water.

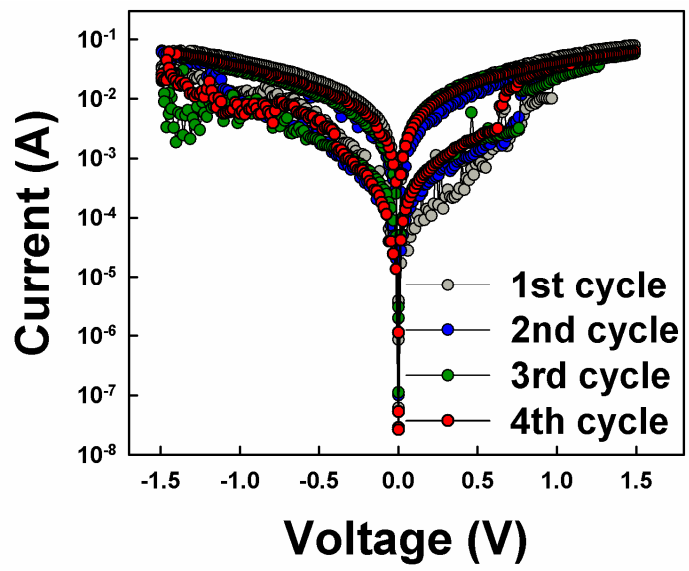

Figure S11. *I-V* curves of (dendrimer/aqueous Fe_3O_4 NP)$_3$ film devices obtained from the repeated operation cycles in the same electrode. The formed multilayers are showed poorer memory performance than prepared in organic media due to leakage current and low particle packing density.

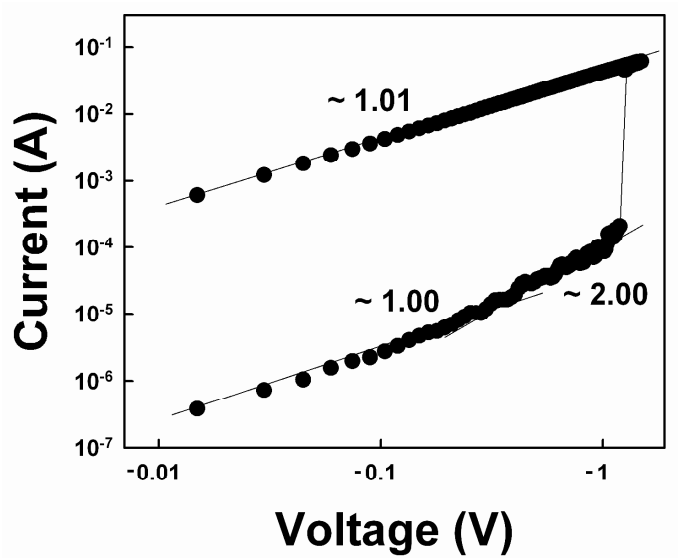

Figure S12. Linear fitting for the *I-V* curve of (dendrimer/OA-Fe_3O_4)$_3$ multilayer devices plotted on a log-log scale during a negative voltage sweep.